the absorbing UV transition, and we take them to bracket the correct answers. In view of the limited accuracy with which the K_i values can be measured, we estimate that these limits are subject to an error of about 5–10° for the larger angles and up to 20–30° for those values of α which are close to zero. In particular, we cannot exclude that both transitions 9 (ν_7) and 11 (ν_9) have transition moments nearly parallel not only to each other but also to the $\pi\pi^*$ transition. Taking the $\pi\pi^*$ transition to be parallel to the Si=C bond, as suggested by the INDO/S calculation which predicts a deviation of 2.5°, permits us to tie the observed transition moment directions to the molecular framework, except that only the absolute values $|\alpha_i|$ are available. In order to assign the signs of these angles, we rely on MNDO calculations (Table II, Figure 6). Their results are those expected by common sense: the Si=C stretch (no. 11, ν_9) and the CH_2 scissoring (no. 9, ν_7) transitions are polarized almost exactly parallel to the Si=C bond, the Si—H stretch (no. 6, ν_5) is polarized parallel to the Si—H bond and the Si—H bend (no. 17, ν_{13}) perpendicular to it, while the symmetrical CH_3 deformation (no. 10, ν_8) is polarized parallel to the Si—C bond and the in-plane CH_3 rock (no. 14, ν_{11}) perpendicular to it. Only the result for the in-plane CH_2 bend, calculated to mix fairly heavily with the SiH bend, is counterintuitive: this vibration is calculated to be polarized nearly parallel to the Si=C bond.

The choice of signs suggested by comparison with the MNDO calculations is shown in Table II. The qualitative agreement between the measured and calculated IR transition moment directions can be seen in Table II and in Figure 6 and is quite satisfactory. Quantitative agreement leaves much to be desired, and it is not obvious which part of the discrepancies is due to experimental inaccuracies and which part to deficiencies of the MNDO model. In particular, although the calculated and measured order of the angles $|\alpha_i|$ agree very well, none of the calculated values are as close to 90° as the measurement suggests.

Still, it is quite remarkable to note how well the approximate experimental IR polarization directions reflect the nature of the vibrational motions assigned previously[3] to the individual IR peaks.

Conclusions

Dimethyldiazidosilane represents a superior photochemical precursor to matrix-isolated dimethylsilylene (**1**) and 1-methylsilene (**2**). Its use permitted us to perform photoselection experiments which established one vibration of **1** as out-of-plane (b_1) and five as in-plane (a_1 or b_2) polarized and four vibrations of **2** as out-of-plane polarized (a″). Most remarkably, a combination of photoselection on two different electronic transitions permitted the assignment of approximate polarization angles to seven in-plane (a′) polarized vibrations of **2**. This represents a potentially very powerful way of characterizing matrix-isolated species. All of the results are in agreement with the IR assignments proposed previously,[3] with MNDO calculations, and with the proposed structures of **1** and **2**. As outlined in more detail elsewhere,[10] we believe that the recent criticism[5,6] of the structural assignment of **1** is unfounded.

Acknowledgment. This work was supported by Air Force Office of Scientific Research Grants F49620-83-C-0044 and 84-0065. One of us (G.R.) is grateful to the Studienstiftung des Deutschen Volkes for a postdoctoral fellowship. We are grateful to Dr. George Radziszewski for help with some of the experiments and to Professor A. C. Arrington (Furman University, Greenville, S.C.), who performed some of the initial work during his sabbatical leave at the University of Utah.

Registry No. **1**, 6376-86-9; **2**, 38063-40-0; dimethyldiazidosilane, 4774-73-6.

The Thermochemistry and Dissociation Dynamics of Internal-Energy-Selected Pyrazole and Imidazole Ions†

Jan Main-Bobo,‡ Susan Olesik,‡ William Gase,‡ Tomas Baer,*‡ Alexander A. Mommers,§ and John L. Holmes§

Contribution from the Department of Chemistry, University of North Carolina, Chapel Hill, North Carolina 27514, and the Department of Chemistry, Ottawa University, Ottawa, Canada.
Received August 26, 1985

Abstract: The two five-membered ring isomers of $C_3H_4N_2^{+\cdot}$, pyrazole and imidazole, have been investigated by photoionization mass spectrometry and photoelectron photoion coincidence spectroscopy. New ionization potentials of 9.25 eV for pyrazole and 8.81 eV for imidazole have been determined from the photoionization efficiency onsets. The dissociation rates of energy-selected ions to the products $CH_2CNH^+ \cdot$ + HCN and $HCNH^+$ + $C_2H_2N\cdot$ have been measured. By comparing these rates with those expected from the statistical theory (RRKM/QET), the 0 K onsets for the dissociation of pyrazole ions have been found to be 11.77 eV ($CH_2CNH^{+\cdot}$) and 11.80 eV ($HCNH^+$). These exceed the thermochemical dissociation limits by 1.25 and 0.85 eV, respectively. The reverse activation barriers are consistent with the measured kinetic energy releases, which are large and nonstatistical. The different dissociation rates and the different branching ratios to the various products demonstrate that pyrazole and imidazole ions do not isomerize to a common structure prior to dissociation. Finally, evidence is presented that shows that electron impact ionization and photoionization produce ions in different manners, which causes the H loss from metastable parent ions to be very intense in electron impact but to be essentially absent in photoionization.

The field of polyatomic ion dissociation dynamics and gas-phase ion structures is an area rich in surprises. Often, the most stable ionic isomer is not stable as a neutral species.[1-5] In addition, some ions can rearrange to lower energy isomeric structures with remarkable facility.[6-10] Among these are the $C_4H_6^{+\cdot}$ isomers:[6] the butadienes, butynes, cyclobutene, and methylenecyclopropane.

† This work has supported by grants from the National Science Foundation and the Department of Energy.
‡ University of North Carolina.
§ Ottawa University.

(1) Holmes, J. L.; Lossing, F. P. *J. Am. Chem. Soc.* **1980**, *102*, 3732.
(2) Burgers, P. C.; Holmes, J. L. *Org. Mass Spectrom.* **1984**, *19*, 452.
(3) Meisels, G. G.; Hsieh, T.; Gilman, J. P. *J. Chem. Phys.* **1980**, *73*, 4126.
(4) Berkowitz, J. *J. Chem. Phys.* **1978**, *69*, 3044.
(5) Holmes, J. L.; Terlouw, J. K. *J. Am. Chem. Soc.* **1979**, *101*, 4973.
(6) Werner, A. S.; Baer, T. *J. Chem. Phys.* **1975**, *62*, 2900.

0002-7863/86/1508-0677$01.50/0

Table I. Ionization and Appearance Energies (eV)

Ion	pyrazole			imidazole		
	IP	AE (298 K)	lit. values	IP	AE (298 K)	lit. values
$C_3H_4N_2^+$	9.25 ± 0.01		9.15,[a,b] 9.27[c]	8.81 ± 0.01		9.12 (EI),[d] 8.78,[a] 8.96[e]
$C_2H_3N^+$		11.76 ± 0.02			11.48 ± 0.02	
CH_2N^+		11.72 ± 0.05			11.67 ± 0.05	

[a] Vertical IP's from PES in ref 23. [b] Vertical IP from PES in ref 24. [c] Adiabatic IP from PES in ref 25. [d] IP from electron impact measurement in ref 15. [e] Vertical IP from PES in ref 26.

Another series of ions that rapidly isomerize at energies below their dissociation limit are the $C_4H_5N^{+\cdot}$ ions: pyrrole, methylacrylonitrile, allyl cyanide, and cyclopropyl cyanide.[7] The members of these two groups of isomeric ions have very different initial structures, but they nevertheless rearrange to common reacting configurations and form identical products.

An important product ion in the dissociation of the pyrrole isomers is $C_2H_3N^{+\cdot}$. As a neutral molecule, the stable structures are methyl cyanide (CH_3CN) and methyl isocyanide (CH_3NC). However, for the ionic species the ketenimine $CH_2CNH^{+\cdot}$ is nearly 3 eV more stable than ionized methyl cyanide and methyl isocyanide.[7] In contrast, the 1,4-dioxane molecular ion does not rearrange to a lower energy isomer (of which there are many) prior to dissociation, and its product structures are not the most stable.[11]

The major reaction channel in the dissociation of pyrazole and imidazole is to $C_2H_3N^{+\cdot}$ + HCN.[12-17] The study of these two ions was undertaken in order to determine whether they rearrange to a common structure prior to dissociation, whether the products

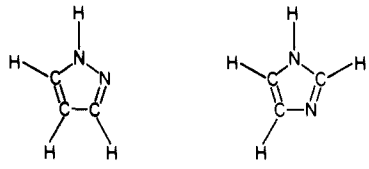

pyrazole imidazole

have the most stable $C_2H_3N^{+\cdot}$ configuration, and whether the reaction kinetics can be well described by the statistical theory. From solely mechanistic considerations, the lowest energy products $CH_2CNH^{+\cdot}$ and HCN can be formed relatively easily from both isomers via a single 1,2-H atom shift preceding fragmentation. Although one might therefore expect that the most stable products would form, other species such as $CHCHNH^{+\cdot}$ and $\overline{CHCHNH}^{+\cdot}$ have nevertheless been proposed.[13-17] Accurate appearance energies for the m/z 41 ion have not been reported, nor have accurate ab initio molecular orbital theory calculations been performed for the relative energies of the $C_2H_3N^{+\cdot}$ isomers. In the present work, the dissociation rates as a function of the ion internal energy, which are extremely sensitive probes of the transition-state structures, as well as their energy, have been measured. In addition, the translational energy released in the dissociation was used to estimate the ground-state energy of the products and therefore their structures. Finally, the structure of the neutral fragments, HCN or HNC, was established.

Experimental Approach

Photoionization Spectrometer and the PEPICO Experiment. The apparatus used to determine photoionization onsets consisted of a hydrogen "many-line" light source that was dispersed by a 1-m vacuum UV monochromator with 200-μm slits, resulting in a photon wavelength resolution of 2 Å (17 meV at 1200 Å). Ions were formed in an ionization region at about 10^{-4} torr, while the vacuum chamber remained at 10^{-6} torr. A quadrupole mass filter was used to analyze the ions. Photoionization efficiency spectra were taken by scanning the monchromator at 1.25 and 0.5 Å/min and collecting the ions for intervals of 40 and 100 s per point, respectively. The photon flux was monitored by converting the vacuum ultraviolet beam to visible radiation by passing it through a sodium salicylate coated window and collecting the light with a photomultiplier.

The photoelectron photoion coincidence (PEPICO) experiment[18] was done by collecting zero-energy electrons in delayed coincidence with the ions. Zero-energy electrons were distinguished from those of higher energy by passing them through a set of collimated holes having a 40:1 aspect ratio. Because the few fragment ions produced had very different masses, the quadrupole mass filter was replaced with an 8-cm-long ion drift region in the coincidence experiment so that the ions were mass analyzed by their time of flight (TOF). Ions were energy-selected by collecing only those ions that were detected in delayed coincidence with (initially) zero-energy electrons. Typical ion signals were 2000 counts/s while the zero-energy electron signal was between 20 and 100 counts/s.

The dissociation rates of the ions were determined by analyzing the time of flight distributions of the fragment ions at selected ion internal energies. Rapidly dissociating parent ions produce fragment ions having symmetric, narrow TOF distributions. On the other hand, slowly dissociating ions (metastable ions) fragment while being accelerated in the 15 V/cm field of the 4-cm-long acceleration region and have asymmetric TOF distributions. The rate is extracted by fitting calculated TOF distributions to those observed experimentally.

Double-Focusing Electron Impact Mass Spectrometer. Kinetic energy release measurements and branching ratios of the various products were carried out with a VG Analytical ZAB-2F double-focusing mass spectrometer in which the ions extracted from the electron impact ion source at 8 kV are mass-selected by a magnetic sector, travel the 1-m length of a field-free region, and are then energy-analyzed by an electric sector. In the mass-analyzed ion kinetic energy (MIKE) experiment, the magnitude and spread of the kinetic energy of fragment ions produced from $C_3H_4N_2^{+\cdot}$ ions in the long field-free region are analyzed by the electric sector. The kinetic energy release distributions (KERD) and average kinetic energy release values were obtained as described elsewhere.[19,20]

Although mass spectrometers have traditionally been used to detect mass-analyzed ions, it is also possible to obtain structural information about the neutral fragments formed in the dissociation of metastable ions.[21,22] When a metastable ion of mass M dissociates in the second field-free region to an ion of mass m and a neutral particle of mass n, the kinetic energy of the parent ion (typically 8 kV) is partitioned among the two fragments according to their mass, i.e., $8m/M$ kV to the ion and $8n/M$ kV to the neutral fragment. By deflecting away the ion beam (which contains the undissociated parent ions and the fragment ions), only the fast-moving neutral particles with energy $8n/M$ pass into the collision cell located near the end of the drift region. Collisional ioni-

(7) Willett, G. D.; Baer, T. *J. Am. Chem. Soc.* **1980**, *102*, 6774.
(8) Stockbauer, R.; Rosenstock, H. M. *Int. J. Mass Spectrom. Ion Phys.* **1978**, *27*, 185.
(9) Smith, D.; Baer, T.; Willett, G. D.; Ormerod, R. C. *Int. J. Mass Spectrom. Ion Phys.* **1979**, *30*, 155.
(10) Baer, T.; Willett, G. D.; Smith, D.; Phillips, J. S. *J. Chem. Phys.* **1979**, *70*, 4076.
(11) Fraser-Monteiro, M. L.; Fraser-Monteiro, L.; Butler, J. J.; Baer, T.; Hass, J. R. *J. Phys. Chem.* **1982**, *86*, 739.
(12) Bowie, J. H.; Cooks, R. G.; Lawesson, S. O.; Schroll, G. *Aust. J. Chem.* **1967**, *20*, 1613.
(13) Hodges, R.; Grimmett, M. *Aust. J. Chem.* **1968**, *21*, 1086.
(14) van Thuijl, J.; Klebe, K. J.; van Houte, J. J. *Org. Mass Spectrom.* **1971**, *5*, 1101.
(15) Klebe, K. J.; van Houte, J. J.; van Thuijl, J. *Org. Mass Spectrom.* **1972**, *6*, 1363.
(16) van Thuijl, J.; van Houte, J. J.; Maquestiau, A.; Flammang, R.; De Meyer, C. *Org. Mass Spectrom.* **1977**, *12*, 196.
(17) Bouchoux, G.; Hoppilliard, Y. *Org. Mass Spectrom.* **1981**, *16*, 459.
(18) Baer, T. In "Gas Phase Ion Chemistry"; Bowers, M. T., Ed.; Academic Press: New York, 1979; Vol. 1, Chapter 5.
(19) Holmes, J. L.; Osborne, A. D. *Int. J. Mass Spectrom. Ion Phys.* **1977**, *23*, 189.
(20) Holmes, J. L.; Osborne, A. D. *Org. Mass Spectrom.* **1981**, *16*, 236.
(21) Burgers, P. C.; Holmes, J. L.; Mommers, A. A.; Terlouw, J. K. *Chem. Phys. Lett.* **1983**, *102*, 1.
(22) Burgers, P. C.; Holmes, J. L.; Mommers, A. A.; Szulejko, J. E.; Terlouw, J. K. *Org. Mass Spectrom.* **1984**, *19*, 442.

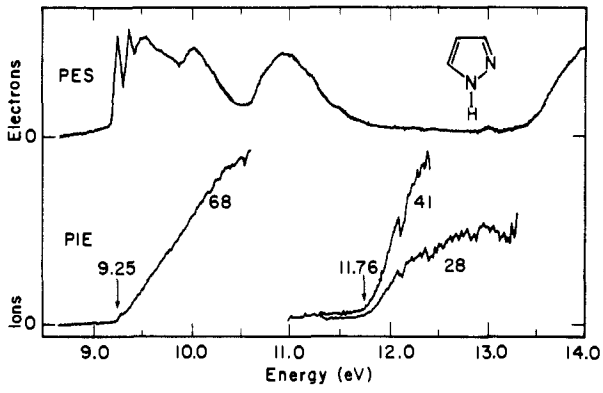

Figure 1. Photoionization efficiency (PIE) spectra for the pyrazole ion (m/z 68) and its fragments. The m/z 41 ion is $C_2H_3N^{+\cdot}$, while the m/z 28 ion is $CNH_2^{+\cdot}$. The photoelectron spectrum (PES) is taken from ref 23.

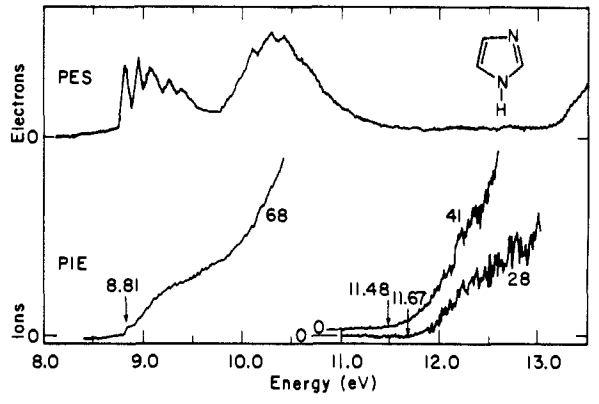

Figure 2. Photoionization efficiency (PIE) spectra for the imidazole ion (m/z 68) and its fragments. The m/z 41 ion is $C_2H_3N^{+\cdot}$, while the m/z 28 ion is $CNH_2^{+\cdot}$. The photoelectron spectrum (PES) is taken from ref 23.

zation, followed by a rapid fragmentation, can be analyzed by the electric sector of the ZAB-2F. In favorable cases, e.g., sufficient flux of neutral particles, the nature of the fragments can be used to determine the structure of the neutral precursor. This technique has been successfully used to show that HCN loss from aniline ions produces HNC rather than the more stable HCN product.[21]

When the ion of interest undergoes several fragmentations on the microsecond time scale, then analysis of the neutral species is complicated by the resulting superposition of the corresponding collisionally induced dissociative ionization (CIDI) mass spectra. The compounds in this study present such a case, as will be seen below.

Pyrazole (98% quoted purity) and imidazole (99% quoted purity) were supplied by the Aldrich Chemical Co. While the pyrazole sample was pure enough to use as is, the imidazole required one or two sublimation operations to remove higher molecular weight impurities.

Results

Photoionization Efficiency (PIE) Spectra. Figures 1 and 2 show the photoionization efficiency (PIE) spectra for pyrazole and imidazole. The sharp onsets for the parent ions (m/z 68) in both spectra made possible the determination of the very accurate ionization energies (given in Table I) from the inflection points of the first steps. In addition, the PIE curves are remarkably free of autoionization features in the initial region, thereby making visible several additional steps that can be associated with onsets to vibrational states of the ions. These steps correlated well with the peaks in the PE spectra[23] shown in Figures 1 and 2.

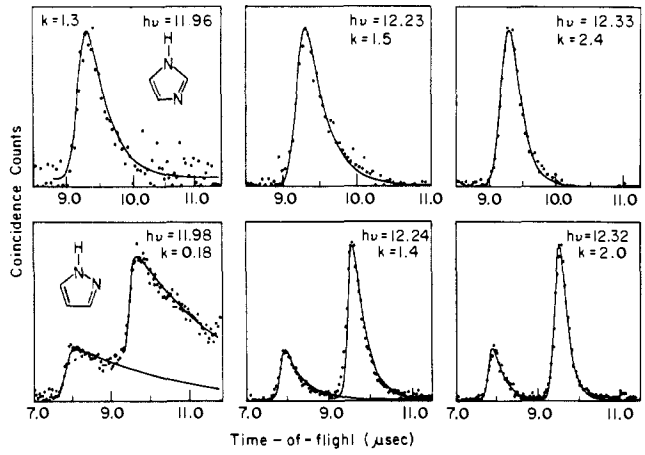

Figure 3. Coincidence time of flight distribution for the fragment ions of imidazole (top) and pyrazole (bottom). The peak at about 8 μs is m/z 28, while the peak at about 9.4 μs is m/z 41. The solid line through the data points are calculated TOF distributions assuming the indicated rates in units of μs^{-1}. The assumed rates of production of m/z 28 and 41 in pyrazole are the same.

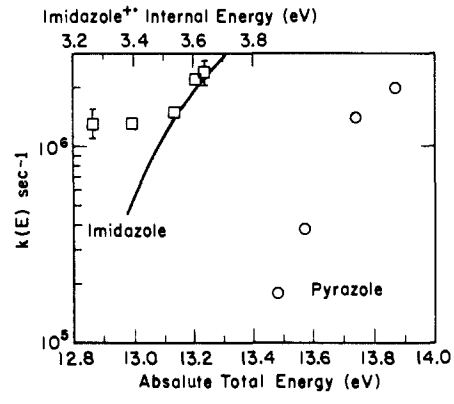

Figure 4. Derived dissociation rates for imidazole and pyrazole ions as a function of the absolute energy [$\Delta H_f°_0$(neutral parent) + hν + E_{th}]. The solid line is the best fit for the RRKM/QET calculation for imidazole assuming an E_0 of 2.78 eV.

The onsets of m/z 41 and 28 occurred at higher energies and were not sharp. Gentle fragment ion onsets can arise for several reasons. If an ion dissociates very slowly at its fragmentation onset, the observed fragment ion signal will not be sharp. However, because the dissociation rate varies approximately exponentially with energy, the first fragment ion to appear ought to be sharp, while subsequent onsets will become progressively less well-defined. In the case of the m/z 41 ion in pyrazole and imidazole, the reason for the gentle onset is that dissociation is taking place in a large Franck–Condon gap region (see the photoelectron spectra in Figures 1 and 2), and, as a result, very few ions are made at this energy. The few that are made result from the decay of autoionizing states, which have been shown to produce zero-energy electrons and vibrationally excited ions.[27] Because of the difficulty in assigning onsets to curves that decay smoothly into the background, the onsets listed in Table I were chosen as the energy at which a straight line through the data points intersect the background signal. However, it must be emphasized that these onsets are only upper limits to the true dissociation limit because of factors such as the transition probability for forming the parent ions at these energies and the reaction' reverse activation energies. A better onset can be determined by modeling the measured dissociation rates with the statistical theory (RRKM/QET).

Lifetimes from PEPICO Data. In order to measure the dissociation rates, PEPICO ion TOF spectra were collected at several

(23) Cradock, S.; Findlay, R. H.; Palmer, M. H. *Tetrahedron* **1973**, *29*, 2173.
(24) Daamen, H.; Oskam, A.; Stufkens, D. J.; Waaijers, H. W. *Inorg. Chim. Acta* **1979**, *34*, 253.
(25) Baker, A. D.; Betteridge, D.; Kemp, N. R.; Kirby, R. E. *Anal. Chem.* **1970**, *42*, 1064.
(26) Ramsey, B. G. *J. Org. Chem.* **1979**, *44*, 2093.
(27) (a) Murray, P. T.; Baer, T. *Int. J. Mass Spectrom. Ion Phys.* **1979**, *30*, 165. (b) Baer, T.; Guyon, P. M.; Nenner, I.; Fouhaille, A. Tabche; Botter, R.; Ferreira, L. F. A.; Govers, T. R. *J. Chem. Phys.* **1979**, *70*, 1585.

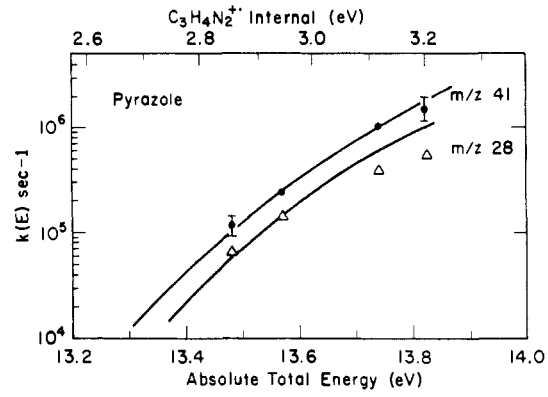

Figure 5. Rates of production of m/z 28 and 41 from pyrazole ions as a function of the ion internal energy. The solid lines are the best fits for the RRKM/QET calculations assuming an E_0 of 2.52 eV.

Table II. Kinetic Energy Release (meV) and Branching Ratios

	$T_{1/2}$[a]	⟨T⟩[b]	metastable peak areas	photoionization at 12.24 eV	PEPICO at 12.02 eV
		Pyrazole Fragments			
$C_3H_3N_2^+ + H\cdot$	330		100	15	c
$CH_2CNH^{+\cdot} + HCN$	90[d]	277	73	100	100
$HCNH^+ + \cdot CH_2CN$	91	200	14	49	56
		Imidazole Fragments			
$C_3H_3N_2^+ + H\cdot$	250		56	13	c
$CH_2CNH^{+\cdot} + HCN$	55[d]	290	100	100	100
$HCNH^+ + \cdot CH_2CN$	84	200	9	73	22

[a] Measured from the peak width at half-height. [b] From the kinetic energy release distribution. [c] Insufficient resolution by TOF to separate m/z 67 and 68. [d] Two-component kinetic energy release.

energies close to the dissociation onsets. For pyrazole, both m/z 41 and 28 products were formed in some abundance. Because of the previously mentioned problem with forming ions with internal energies in the Franck–Condon gap, only the m/z 41 fragment ions from imidazole were sufficiently intense for analysis. The m/z 28 ion peak was considerably less intense in imidazole than it was in pyrazole. Figure 3 shows some of the TOF distributions and the calculated fits through the data points. All data sets were fitted adequately by assuming single-exponential decays. This indicated that if these ions isomerize to lower energy structures, they do so at rates that are much faster than the dissociation rates.

The rate vs. total energy curves derived from analysis of these data are shown in Figure 4. The total energy is the 0 K heat of formation of the neutral molecule plus the photon energy plus the average thermal energy of the molecule, which is 128 meV. By plotting the data for the two ions in this manner, it is readily evident that these two ions do not isomerize to a common structure prior to dissociation because their dissociation rates differ by a factor of about 100. This conclusion is consistent with other data, such as the kinetic energy released, the different branching ratios, and the large reverse activation energies.

In the case of pyrazole, the total dissociation rates were determined from either the m/z 28 or the 41 fragment TOF distribution (Figure 3). The rates for forming each fragment separately were then derived from the respective peak area. The individual rates are shown as a function of the ion internal energy in Figure 5.

Kinetic Energy Release Results. The release of kinetic energy in a dissociation reaction results in a symmetric broadening of the PEPICO fragment ion TOF distribution. However, this broadening is not easily analyzed in the presence of the additional asymmetric broadening caused by slow dissociation of the parent ions. Accordingly, the translational energies released from metastable ions decomposing in the second field-free region of a ZAB-2F mass spectrometer were measured, and the results are given in Table II. The products were formed with considerable

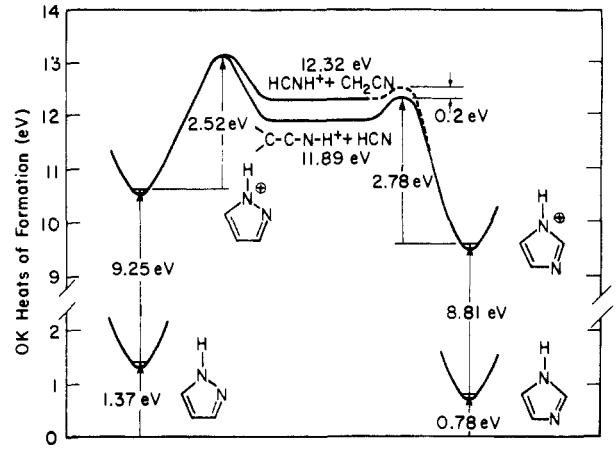

Figure 6. Thermochemistry for the dissociation reactions of pyrazole and imidazole ions.

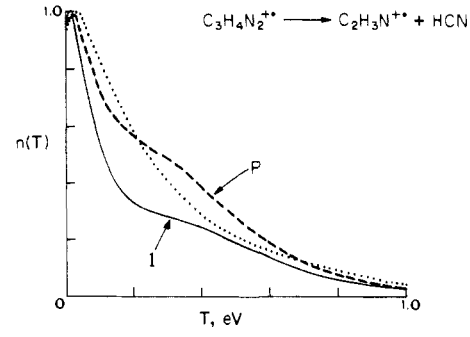

Figure 7. Bimodal kinetic energy release distributions (KERDs) for the m/z 68 → m/z 41 fragmentation of ionized pyrazole (P) and Imidazole (I). The dotted third line is for a noncomplex Gaussian type metastable peak $h/h_0 = \exp[-\ln 2w^{1.5}]$ (see text) and average kinetic energy release of 300 meV.

release of kinetic energy, which is in keeping with the threshold appearance energy measurements for the reactions, summarized in Figure 6, all of which require energy appreciably in excess of the thermochemical threshold.

The metastable peaks for H-atom loss from both compounds were steep sided with flat tops, typical of reactions having reverse energy barriers[28] and in which a large fraction of the excess internal energy of the fragmenting ions is partitioned among translational degrees of freedom.

The peaks for formation of m/z 41 were of Gaussian type, but neither could be fitted to the modified Gaussian equation[20] $h/h_0 = \exp[-\ln 2w^n]$, where h/h_0 is the fraction of the peak height at which the width w is measured. The exponent, n, which is equal to 2 for a true Gaussian function, is an adjustable parameter. The KERD expected for the modified Gaussian function with $n = 1.5$ is compared in Figure 7 with the experimental results. The pyrazole and imidazole dissociations clearly have complex KERDs. These bimodal KERDs show that two reaction paths are involved for ions fragmenting on the microsecond time scale. Bimodal KERDs can arise from the production of two daughter ion structures with a single or two different reacting configurations or from the generation of a single daughter ion via two transition states. To investigate the former possibility the collision-induced decomposition (CID) and charge-stripping (CS) mass spectra and the Xe/He neutralization–reionization mass spectra (NRMS)[29] of the m/z 41 daughter ions were carefully compared. No significant differences could be discerned between the corresponding spectra of the m/z 41 ions from the isomeric percursor molecules, and so it was concluded that a single daughter ion is almost certainly generated. It was noted that the CID and NRMS of

(28) Holmes, J. L.; Terlouw, J. K. *Org. Mass Spectrom.* **1980**, *15*, 383.
(29) Terlouw, J. K.; Kieskamp, W. M.; Holmes, J. L.; Mommers, A. A.; Burgers, P. C. *Int. J. Mass Spectrom. Ion Processes* **1985**, *64*, 245.

imidazole and pyrazole molecular ions are significantly different in that the latter produces peaks at m/z 36 and 37 (from $C_3^{+\cdot}$ and C_3H^+ ions) that are completely absent for the former, showing that imidazole molecular ions that have insufficient energy to fragment in the microsecond time scale do not rearrange to $[pyrazole]^{+\cdot}$. It seems likely therefore, that the m/z 41 daughter ions are produced via two transition states for each $[C_3H_4N_2]^{+\cdot}$ isomer. Each KERD contains different large and small kinetic energy release components, and it is proposed that the large energy release component arises from the fragmentation whose appearance energy has been measured in the photon-induced dissociations.

Structure of Neutral Fragments. The neutral fragment accompanying the m/z 41 ion may be either HCN or HNC, the excess energy for the fragmentations being sufficient to accommodate the high-energy isomer (Figure 6). These neutral molecules can in principle readily be identified by means of their CIDI (collision-induced dissociative ionization) mass spectra in the region m/z 12–16.[21] Unfortunately, the ion flux from metastable fragmentation is only about 3×10^{-4} as great as the incoming $C_3H_4N_2^{+\cdot}$ flux, and so the low-mass region of the CIDI mass spectrum is too weak for quantitative analysis, although for both precursors m/z 13 was clearly more intense than m/z 12, indicating that HCN is the likely neutral species. Accordingly, the m/z 24–28 region was used instead. Danis et al.[30] recently reported m/z 26:27 ratios for the CIDI characteristics of HCN and HNC of 1.5 and 0.8, respectively. In the modified ZAB-2F mass spectrometer, under single-collision conditions, the above ratios were measured as 0.24 (HCN from $C_6H_5CN^{+\cdot}$) and 0.13 (HNC from $C_6H_5NH_2)^{+\cdot}$). The reason for this difference from the earlier[30] observations is not clear, but it should be noted that stronger signals can be generated by raising the ionizing collision gas (He) pressure to multiple collision conditions, but, then, as a result of diffusion of He from the collision cell into the field-free region, extra and different neutral species are generated by *collision-induced* decomposition of the mass-selected precursor ions. For the aromatic compounds benzonitrile and aniline this effect manifests itself by the appearance of m/z 24 and 25 (absent under single-collision conditions), and the m/z 26:27 ratio rises rapidly due to the presence of collisionally generated C_2H_2.

For pyrazole and imidazole, identification of the neutral fragments accompanying $C_2H_3N^+$ is only slightly complicated by the cogeneration of $CH_2CN\cdot$ radicals (see Table II) because the latter are relatively less abundant. For both compounds interference from CH_2CN was slight and the corrected m/z 26:27 ratios were 0.25 ± 0.03, showing that HCN is indeed the neutral product.

Branching Ratios to the Various Products. Metastable ions in the ZAB-2F mass spectrometer are those ions that decompose ca. 10 μs after their generation in the ion source. From the data of Figures 4 and 5, it can be deduced that these are pyrazole and imidazole ions that have an internal energy of about 12 eV. (The fact that they are both 12 eV is purely coincidental, the result of two opposing factors.) The branching ratios of the metastable ions in the ZAB-2F are listed in Table II along with the branching ratios obtained from the photoionization and PEPICO experiment at energies between 12.02 and 12.24 eV. The two sets of data are not strictly comparable because the fragments from the metastable ions come from parent ions that are internal-energy-selected (by the time scale of the observations), whereas the fragments in the photoionization data come from parent ions that are not energy-selected. On the other hand, the photoionization data at 12.2 eV involves parent ions whose energies are limited between the photon energy and the dissociation limits of 11.77 and 11.59 eV respectively for pyrazole and imidazole. In addition, the quadrupole mass filter tends to discriminate against higher mass ions. Finally, the PEPICO branching ratios are truly state-selected branching ratios. However, only the m/z 41 and 28 ions could be resolved by time-of-flight.

(30) Danis, P. O.; Wesdemiotis, C.; McLafferty, F. W. *J. Am. Chem. Soc.* **1983**, *105*, 7454.

Table III. Thermochemistry (kJ/mol) of Selected Neutral Particles and Ions

molecule or ion	$\Delta H_f^\circ{}_{298}$	$\Delta H_f^\circ{}_0$
$C_3H_4N_2$ (pyrazole)	116.0[a]	132.0[b]
$C_3H_4N_2$ (imidazole)	58.6[a]	74.9[b]
$C_3H_4N_2^{+\cdot}$ (pyrazole)	1011[c]	1027[c]
$C_3H_4N_2^{+\cdot}$ (imidazole)	911[c]	928[c]
$HCNH^+$	941[d]	939[b]
$CH_2CN\cdot$	246[e]	253[b]
HCN	135[f]	136[b]
HNC	196[b]	197[g]
$CH_2CNH^{+\cdot}$	1004 ± 7[h]	1011 ± 7[b]
$CH_2NCH^{+\cdot}$	1045[b]	1052 ± 25[i]
$CH_3CN^{+\cdot}$	1263[b]	1270 ± 3[j]
$CH_3NC^{+\cdot}$	1233[b]	1240 ± 3[j]
$\overline{CHCHNH}^{+\cdot}$	1238[b]	1245 ± 20[i]
$CHCHNH^{+\cdot}$	1285[b]	1292 ± 20[i]

[a] Reference 35. [b] Converted from 298 K or 0 K values with the procedure described in ref 11 and frequencies in Table IV. [c] This work. [d] Reference 36. [e] References 37 and 38. [f] Refernece 39. [g] Reference 43. [h] Experimental energy from ref 7. Structure was verified by ab initio calculations at the 3-21G and 4-31G levels. [i] This energy was calculated by ab initio techniques at either the 4-31G and/or the 3-21G levels and compared to the calculated (and known) ΔH_f° of $CH_3CN^{+\cdot}$. [j] Reference 40.

The branching ratios obtained by electron impact and photoionization are very different, the low probability for H loss in photoionization being particularly striking. It is reminiscent of the complete lack of H loss in the photoionization of $CH_3Cl^{+\cdot}$ at its thermochemical onset,[31,32] while the onset is easily observed by electron impact ionization. Because the $C_3H_4N_2^{+\cdot}$ ions are metastable at energies that fall in the Franck–Condon gap (see PES in Figures 1 and 2), they must have resulted from autoionization of excited neutral molecules. It is well-known[34] that electron impact can produce excited states not accessible by photon excitation, such as triplet states. Thus, pyrazole and imidazole appear to be two more examples in which such an effect is operative.

Discussion

Ion and Neutral Fragment Structures and Thermochemistry. The 298 K heats of formation of the neutral pyrazole and imidazole molecules are well established. The corresponding ionic heats of formation can therefore be obtained from the measured ionization potentials (see Table III). As pointed out previously, the sharp steps at the ionization onsets provide very reliable ionization potentials, which are listed in Table I. These differ somewhat from previous PES measurements for reasons that are not clear. The present onsets can be calibrated against the Lyman α line of the light source and are therefore accurate to ±0.010 eV. The 298 K heats of formation were converted to 0 K values by the methods previously discussed in detail.[11] Vibrational frequencies (Table IV) of the pyrazole and imidazole molecules were used for both the neutral and ionized species. Figure 6 shows the 0 K ion thermochemistry constructed from these data together with the dissociation limits and transition-state energies that were determined by RRKM/QET calculations, as discussed in the next section.

(31) (a) Werner, A. S.; Tsai, B. P.; Baer, T. *J. Chem. Phys.* **1974**, *60*, 3650. (b) Baer, T.; Werner, A. S.; Tsai, B. P.; Lin, S. F. *J. Chem. Phys.* **1974**, *61*, 5468.

(32) Eland, J. H. D.; Frey, R.; Kuestler, A.; Schulte, H.; Brehm, B. *Int. J. Mass Spectrom. Ion Phys.* **1976**, *22*, 155.

(33) Lossing, F. P. *Bull. Soc. Chim. Belg.* **1972**, *81*, 125.

(34) Trajmar, S.; Williams, W.; Kupperman, A. *J. Chem. Phys.* **1973**, *58*, 2521.

(35) Pedley, J. B.; Rylance, J. "Sussex-N.P.L. Computer Analyzed Thermochemical Data: Organic and Organo metallic Compounds"; University of Sussex Sussex, UK, 1977.

(36) Wolf, J. F.; Staley, R. H.; Koppel, I.; Taagepera, M.; McIver, R. T., Jr.; Beauchamp, J. L.; Taft, R. W. *J. Am. Chem. Soc.* **1977**, *99*, 5417.

(37) Benson, S. "Thermochemical Kinetics", 2nd ed.; Wiley: New York, 1979; p 299.

The major reaction channel leads to $C_2H_3N^{+\cdot}$ + HCN. The lowest energy isomers of these products, shown in Figure 6, have the structures $CH_2CNH^{+\cdot}$ and HCN.[7] Their 0 K energies, relative to the neutral molecules of pyrazole and imidazole, are 10.52 eV and 11.11 eV, respectively, both considerably below their respective appearance energies of 11.76 eV and 11.48 eV. Although it is possible that isomeric higher energy products are formed, it seems unlikely in view of the simple bond cleavages that may be proposed as leading to these lowest energy isomers. Nevertheless, several investigators have proposed other $C_2H_3N^{+\cdot}$ isomers as possible products.[16,17]

As a result of these questions, the energies of six of the most likely $C_2H_3N^{+\cdot}$ isomers were considered (see Table III). Only two of these, $CH_3CN^{+\cdot}$ and $CH_3NC^{+\cdot}$, have experimentally known heats of formation. The energies of the other isomers listed in Table III have been calculated by the GAUSSIAN 82 ab initio program. Geometry optimization was performed at the STO-3G level, while the energies were determined at the 3-21G level. The results compared favorably with previous calculations[7] using the 4-31G basis set.

It is possible on energetic considerations alone to rule out the production of the following $C_2H_3N^{+\cdot}$ isomers: $CH_3CN^{+\cdot}$, $CH_3NC^{+\cdot}$, $CHCHNH^{+\cdot}$, and $\overline{CHCHNH}^{+\cdot}$. The formation of these ions from $[pyrazole]^{+\cdot}$ or $[imidazole]^{+\cdot}$ could only occur 1 eV in excess of the experimentally determined onset. This leaves only the two closely related ions, $CH_2CNH^{+\cdot}$ and $CH_2NCH^{+\cdot}$. The former has a structure analogous to the very stable allene ion $(CH_2CCH_2)^{+\cdot}$) and is expected to be the most stable $C_2H_3N^{+\cdot}$ ion, as was indeed found. However, the $CH_2NCH^{+\cdot}$ structure, which has a calculated energy only 0.43 eV above the $CH_2CNH^{+\cdot}$ structure, is an energetically possible product ion. On the other hand, it is a somewhat unlikely product for these two dissociation reactions. The CID measurements indicated that the same m/z 41 product ion is formed from both pyrazole and imidazole. In the case of pyrazole with its two adjacent nitrogen atoms, it is impossible to produce $CH_2NCH^{+\cdot}$ without considerable rearrangement of the carbon and nitrogen atoms, a process that is highly unlikely in view of the dissociation rate data. This leaves only the $CH_2CNH^{+\cdot}$ ion as both the energetically most stable and the mechanistically most readily produced product structure.

Although there appears to be only one $C_2H_3N^{+\cdot}$ isomer generated in the metastable time and energy region, the higher energy (by 0.63 eV[34]) HNC neutral molecule would be consistent with the reaction energetics. However, this structure is deemed to be absent on the basis of the CIDI observations.

Because of the reverse activation energy, the ground-state ion energies are unobtainable from the onset measurements. The measured translational energy released represents only part of the reverse activation energy. Without a considerable knowledge of the potential energy surface for the dissociation reaction, it is not possible to determine what fraction of the total excess energy is released into translational degrees of freedom. Even with the assumption that energies are distributed statistically, further progress is barred by the bimodal kinetic energy release distributions, the origins of which are not known with certainty.

The RRMK/QET Calculated Rates. Figures 4 and 5 show the measured and calculated dissociation rates. Neither the activation energy, E_0, nor the transition-state structures are known, and so the rates were calculated for several values of E_0 by assuming that the vibrational frequencies are the same in the transition state and molecular ion. This latter assumption is justified because there is a reverse activation energy, causing the transition-state structure to be "tight". A measure of the tightness can be obtained from the assumed $\Delta S^{\ddagger}$, which is $k \ln [\prod q_i^{\ddagger}/\prod q_i]$, where the q_i's are the vibrational partition functions. A $\Delta S^{\ddagger}$ of 0 would mean that the vibrational frequencies of the transition state and the molecular ion are the same and that the two are similar in structure. In most simple bond cleavage reactions $\Delta S^{\ddagger}$ is between 8 and 15 cal mol^{-1} K^{-1}. The best fits in Figures 4 and 5 were obtained, however, for $\Delta S^{\ddagger}$ values of -1 cal mol^{-1} K^{-1}, which is characteristic of a tight complex. A transition state consistent with this $\Delta S^{\ddagger}$ is one in which the ring structure is preserved and some additional strain is introduced, perhaps in the form of a hydrogen transfer step. It is sometimes possible to compare the reaction A factors, $(kT/h)\exp(\Delta S^{\ddagger}/R)$, for ionic and neutral reactions. In this case the A factor at a temperature of 1000 K is calculated to be $10^{13.2}$. Unfortunately, there are no corresponding neutral reactions that yield these products.

The above conclusion is consistent with the kinetic energy release data. Because the translational energy distribution for the loss of HCN from pyrazole is rather broad, the reaction, once having passed through the tight transition state, is still far from simple. There must be additional nuclear motions that distribute the available excess energy among the vibrational degrees of freedom.

The imidazole dissociation is more complicated than that of pyrazole in that the rate data in Figure 4 show an atypical dependence on the ion internal energy. First, at the lowest energies, the rate seems to be independent of the ion internal energy. The only effect of lowering the ion internal energy was to decrease the signal. Yet, the rate ought to be much lower than is suggested by the data. Finally, it is important to reiterate that the fragment ion signal is very weak because parent ions cannot be formed by direct ionization in this Franck–Condon gap region, and thus the fragmenting metastable ions are certainly formed by autoionization. It is possible that in the case of imidazole, autoionization does not produce ions below a total energy of 13 eV. Thus, as the photon energy is lowered, thermally excited imidazole molecules are being ionized that yield ions of the same total energy independent of the photon energy. This would explain the constant, and high, rate of dissociation of the imidazole ions at low internal energies.

The bimodal KERDs and the apparent production of a single m/z 41 product ion indicate that both reactions proceed via two or more transition states, possibly with slightly different activation energies. Because only the total dissociation rate is reflected in the rate data of Figure 3, it is not possible to learn more about the bimodal KERDs from these measurements. On the other hand, the RRKM/QET calcultions are affected by the presence of several decay channels. Were these to be included in the model, the assumed frequencies for the transition state would have to be increased, thereby making the transition state tighter still. However, the effect is small so that it would not shed additional light on the problem of multiple transition states.

Fragmentation Mechanism. On the basis of all the observations, it is possible to make proposals concerning the fragmentation mechanisms. Of major interest is the nature of the transition state for the HCN loss. Does the rate-determining step involve an H-atom transfer, or a bond rupture? Does one transition state serve for both polyatomic product channels to m/z 41 and 28, or are they separate? A comparison of the activation energies for the two product channels for pyrazole and imidazole shows that in pyrazole they have nearly identical onsets, even though the final product energies are very different. On the other hand, the two activation energies are different in the case of imidazole. On the basis of this observation as well as the fact that the ion must "loosen up" after the transition state in order to dissociate with a broad distribution of kinetic energy releases, we propose the following mechanism. In pyrazole, the critical reaction coordinate is the C–C bond, which breaks in the transition state.

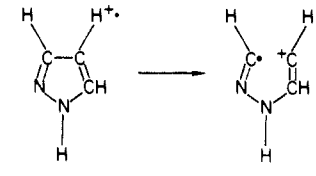

The products then depend upon simple 1,2-H shifts, one for the generation of $C_2H_3N^{+\cdot}$.

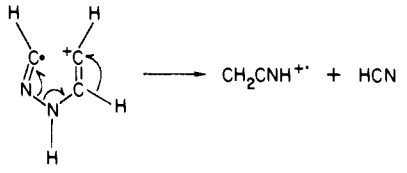

and a second for $HCNH^+$ formation

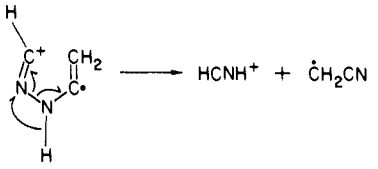

In the case of ionized imidazole, the C–C bond is formally a double bond and therefore stronger than in pyrazole. The candidates for ring opening are then the other three C–N bonds. If H-atom transfer between the two nonadjacent nitrogen atoms is ignored, the breaking of two of the C–N bonds will lead to HCN loss, while breaking the remaining C–N bond can lead to loss of CH_2CN.

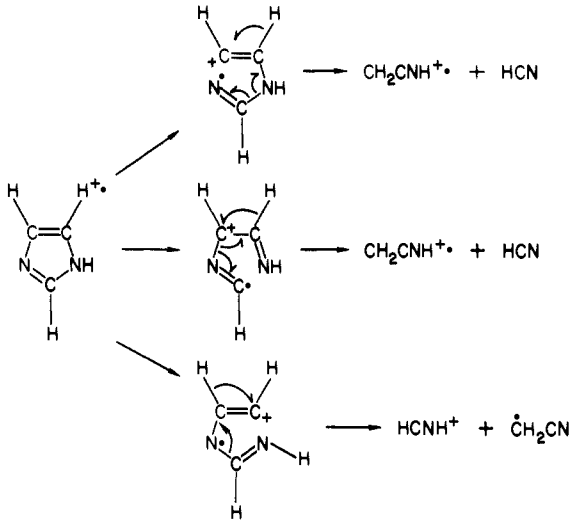

Although the tautomeric H-atom shift between the two N atoms probably takes place in the molecule and ion, it may be prohibited in the transition state because at the threshold all the energy is used up in the 1,2-H atom transfer from C to C and in the initial stages of the C–N bond-breaking step. The three C–N bond-breaking steps are not equivalent, and it is to be expected that the three transition states will have somewhat different energies because the corresponding bond energies are not equivalent.

These transition-state models can account not only for the different activation energies for HCN and CH_2CN loss from imidazole but also for the two component kinetic energy releases that we have observed for HCN loss. Furthermore, the model predicts only a single pathway to m/z 28, which is indeed in keeping with the observed kinetic energy release having only a single component. However, the model does not account for the bimodal KERD in the HCN loss from pyrazole ions.

We have not discussed the reaction for H-atom loss. This is because we have no data other than the kinetic energy release. We know neither the onset energy nor the structure of the resulting $C_3H_3N_2^+$ ion. As a result, we cannot shed new light on this reaction path.

Table IV. Vibrational Frequencies Used in RRKM/QET Calculations and Thermochemical Conversions

		$C_3H_4N_2^{+\cdot}$ Molecular Ion[a]			
3500 (1)	3130 (3)	1500 (2)	1340 (4)	1110 (4)	900 (1)
850 (2)	745 (1)	650 (2)	520 (1)		
		Pyrazole Transition State			
3500 (1)	3130 (3)	1500 (2)	1340 (3)	1110 (4)	900 (3)
745 (1)	680 (3)				
		Imidazole Transition State			
3500 (1)	3130 (3)	1500 (2)	1340 (3)	1110 (4)	900 (3)
800 (1)	700 (3)				
		$CH_2CNH^{+\cdot}$[b]			
3300 (1)	3000 (2)	1450 (1)	1380 (1)	1100 (1)	940 (1)
825 (1)	360 (1)				
		$HCNH^+$[b]			
3460 (1)	3150 (1)	2180 (1)	870 (1)	700 (1)	
		CH_2CN[b]			
3000 (2)	2270 (1)	1420 (2)	920 (1)	360 (2)	

[a] The neutral pyrazole and imidazole frequencies (ref 41) were rounded off for calculational purposes. Degeneracies are listed in parentheses. [b] Estimated from the vibrational frequencies of neutral CH_3CN (ref 42).

Registry No. Pyrazole, 288-13-1; imidazole, 288-32-4.

(38) King, K. D.; Goddard, R. D. *Int. J. Chem. Kinet.* **1975**, *7*, 837.
(39) Wagman, D. D.; Evans, W. H.; Parker, V. B.; Halow, I.; Bailey, S. M.; Schumm, R. H. "Selected Values of Chemical Thermodynamic Properties. Tables For First Thirty-Four Elements in the Standard Order Arrangement"; N.B.S. Technical Note 270-3, U.S. Government Printing Office: Washington, D.C., 1968.
(40) Rosenstock, H. M.; Draxl, K.; Steiner, B.; Herron, J. T. *J. Phys. Chem. Ref. Data Suppl.* **1977**, *6*, 1.
(41) Tabacik, V.; Pellegrin, V. *Spectrochim. Acta* **1979**, *35A*, 1055.
(42) Dewar, M. J. S.; Ford, G. P. *J. Am. Chem. Soc.* **1977**, *99*, 1685.
(43) Pearson, P. K.; Schaefer, H. F.; Wahlgren, V. *J. Chem. Phys.* **1975**, *62*, 350.